Rearrangements under confinement lead to increased binding energy of Synaptotagmin-1 with anionic membranes in Mg^{2+} and Ca^{2+}

Clémence Gruget,[1] Jeff Coleman,[2] Oscar Bello,[3] Shyam S. Krishnakumar,[2,3] Eric Perez,[1] James E. Rothman,[2,3] Frederic Pincet,[1,2,*] Stephen H. Donaldson Jr.[4,*]

[1]Laboratoire de Physique Statistique, Ecole Normale Supérieure, PSL Research University, 24 rue Lhomond, 75005 Paris, France

[2]Department of Cell Biology, Yale University School of Medicine, New Haven, CT, 06520 USA

[3]Department of Clinical and Experimental Epilepsy, Institute of Neurology, University College London, London, United Kingdom

[4]Département de Physique, Ecole Normale Supérieure, PSL Research University, CNRS, 24 rue Lhomond, 75005 Paris, France

*Corresponding authors, pincet@lps.ens.fr and steve.donaldson@phys.ens.fr

Abstract

Synaptotagmin-1 (Syt1) is the primary calcium sensor (Ca^{2+}) that mediates neurotransmitter release at the synapse. The tandem C2 domains (C2A and C2B) of Syt1 exhibit functionally-critical, Ca^{2+}-dependent interactions with the plasma membrane. With the surface forces apparatus, we directly measure the binding energy of membrane-anchored Syt1 to an anionic membrane and find that Syt1 binds with ~6 k_BT in EGTA, ~10 k_BT in Mg^{2+}, and ~18 k_BT in Ca^{2+}. Molecular rearrangements measured during confinement are more prevalent in Ca^{2+} and Mg^{2+} and suggest that Syt1 initially binds through C2B, then reorients the C2 domains into the preferred binding configuration. These results provide energetic and mechanistic details of the Syt1 Ca^{2+}-activation process in synaptic transmission.

1. Introduction

Upon arrival of an action potential at the neuronal synapse, calcium ions (Ca^{2+}) enter the cytosol of the neuron, triggering the soluble N-ethylmaleimide-sensitive factor activating protein receptor (SNARE) proteins to fully zipper, leading to fusion of pre-docked vesicles containing neurotransmitters [1,2]. Synaptotagmin-1 (Syt1), a synaptic vesicle associated protein, has been identified as the principal Ca^{2+} sensor that activates SNAREs following Ca^{2+} influx [1,3,4]. Syt1

has two Ca^{2+} binding C2 domains (C2A and C2B), connected by a 9-residue flexible linker domain, and a 61-residue linker domain between the transmembrane domain and the tandem C2 domains. Syt1 is known to interact with the plasma membrane both before and after Ca^{2+} binding. A polylysine stretch in C2B has been shown to interact with anionic lipids in the absence of Ca^{2+} [5–8]. Upon Ca^{2+} influx, three Ca^{2+} bind in C2A and two Ca^{2+} bind in C2B. Ca^{2+} binding to the anionic pocket effectively neutralizes electrostatic repulsion between the binding site and the target membrane [9], which allows non-polar residues nearby the Ca^{2+} binding sites (also referred to as hydrophobic loops) to insert into the membrane [9–12], serving as the power stroke to activate fusion.

The precise biochemical and biophysical mechanisms for the Syt1 Ca^{2+}-trigger remain unclear. While mutating the C2A Ca^{2+} binding site causes a significant decrease to evoked neurotransmitter release *in vivo*, an analogous mutation in C2B effectively abolishes evoked release [13,14]. Several studies illustrate that Syt1 can oligomerize and modulate bending of the target membrane, and that C2B drives these processes [4,15,16]. Syt1 is therefore thought to function at least partially by performing bending work on the target membrane, providing a highly curved membrane to ease the high energy barrier associated with membrane fusion. Syt1 may also act as a clamp in the absence of Ca^{2+}, by forming oligomerized structures which keep the SNAREs away from the vesicle-membrane contact zone [16–19].

The kinetics and assembly of soluble C2AB (*i.e.*, Syt1 without the transmembrane domain and linker domain, containing only the soluble C2A and C2B domains) with anionic membranes have been assessed using stopped-flow fluorescence resonance energy transfer (FRET) and microscale thermophoresis (MST) measurements, revealing strong binding between soluble C2AB and membranes containing phosphatidylserine (PS) and phosphatidylinosotinol (PIP2) in the absence of Ca^{2+}, attributed to the polybasic patch binding to PIP2/PS [6,9]. The presence of PIP2 leads to an increase in the Ca^{2+} affinity of Syt1, possibly due to conformational changes induced by PIP2 binding [6]. Ca^{2+} binding by Syt1 also leads to a large decrease in the off-rate of Syt1 from membranes [9], presumably due to insertion of the non-polar residues in the C2AB Ca^{2+} binding loops. A recent paper measured energetics of single-molecule C2AB interactions with optical tweezers in the presence of Ca^{2+} [20], but reported a lack of binding in the absence of Ca^{2+}. A previous single-molecule AFM study attached Syt1 to an AFM tip and performed adhesion force

measurements at PC/PS membranes [21], but no binding energetics or distance-dependent Syt1-membrane interactions were reported. Additionally, while Mg^{2+} is known to bind in the Syt1 Ca^{2+}-binding sites in the absence of Ca^{2+} [22] and has subtle effects on Syt1-membrane interactions [23,24], no studies have directly compared the binding energies in Mg^{2+} and Ca^{2+}. Therefore, there remains a lack of direct probes of the long-range and short-range behaviors and energetics of divalent ion-dependent Syt1 binding at anionic membranes, especially with Syt1 embedded in a membrane, as occurs under physiological conditions.

We directly measured the interaction energy between a lipid membrane decorated with the cytoplasmic portion of Syt1 and an anionic membrane composed of PC/PS/PIP2 using a surface forces apparatus (SFA), as shown schematically in Figure 1. To isolate the Syt1-target membrane interaction, which has been shown to be more productive for fusion [5,24–26], we have included only PC and Syt1 in the protein-containing membrane. By using EGTA, Mg^{2+}, or Ca^{2+} in the buffer, the effects of divalent ions are elucidated during Syt1 confinement, docking, and unbinding at an anionic membrane surface, including binding energetics, kinetics, and molecular rearrangements.

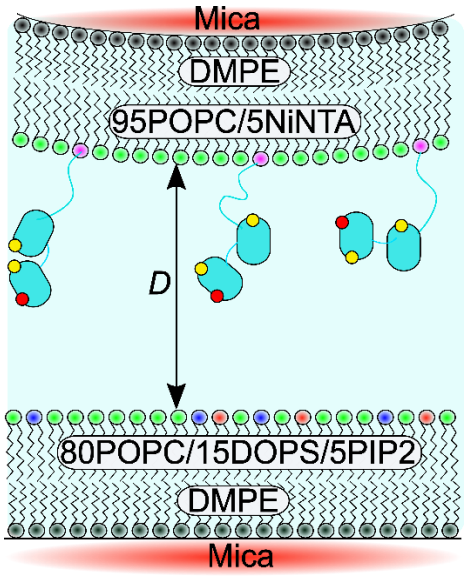

Figure 1. A schematic of the SFA experiment. Syt1 coated membrane (top) interacts with an anionic membrane (bottom), consisting of 80mol% POPC, 15mol% DOPS, and 5mol% PIP2. The Ca^{2+} binding loops of C2A and C2B are indicated by the yellow sites, and the polybasic patch on C2B is indicated by the red site.

2. Materials and Methods

2.1. Protein expression and purification

The DNA construct used in this study was generated by cloning the cytoplasmic domain (residues 83 to 421) of rat synaptotagmin-1 into pGEX6p-1 (GE Healthcare, Marlborough, MA) using restriction sites XhoI and NotI. A 12x histidine residue tag was added upstream (N-terminal of the protein) using BamHI and XhoI. Two residues, C277A and E269C, were mutated using a QuikChange mutagenesis kit (Agilent Technologies, Santa Clara, CA) to allow for subsequent fluorescent labelling. The construct was transformed and grown in Escherichia coli BL21(DE3) to an OD 600 ~0.8 and the expression was induced with 0.5 mM isopropyl b-D-1-thiogalactopyranoside (IPTG). The cells were harvested after 4 hr at 37˚C and suspended in lysis buffer (25 mM HEPES, pH 7.4, 500 mM KCl, 1 mM $MgCl_2$, 1 mM $CaCl_2$, 15mM Imidazole, 0.4 mM TCEP, 10% glycerol, 1% Triton X-100, protease inhibitors). The sample was lysed using a cell disrupter, and the lysate was supplemented with 0.1% polyethylimine before centrifugation (35,000 rpm for 30 min). The supernatant was loaded onto Ni-NTA (Qiagen, Valencia, CA) beads (3-4 hours or overnight at 4˚C) with 10 ul of Benzonase (2000 units). The beads were washed with 20mL of lysis buffer with 0.1% Triton X-100, then re-suspended in 5ml of lysis buffer supplemented with 10 μg/mL of DNAse I, 10 μg/mL of RNAseA and 10μl of Benzonase, and incubated at room temperature for 1 hour.

Subsequently, the beads were rinsed quickly with 10 mL of high salt buffer (25 mM HEPES, pH 7.4, 1M KCl, 1 mM $MgCl_2$, 1 mM $CaCl_2$, 15mM Imidazole, 0.4 mM TCEP, 10% glycerol) to remove nucleotide contamination, and washed several times with 25 mM HEPES, pH 7.4, 500 mM KCl, 50mM Imidazole, 1 mM $MgCl_2$, 1 mM $CaCl_2$, 0.4 mM TCEP, 10% glycerol. The protein was eluted off the nickel beads in 25 mM HEPES, pH 7.4, 400 mM KCl, 500 mM Imidazole, 0.5 mM $CaCl_2$, 0.4 mM TCEP, 10% glycerol. The GST tag was cleaved overnight at 4°C using Prescission protease, and then removed with a 1 hour room temperature incubation in Glutathione-Sepharose (Thermo Fisher Scientific, Grant Island, NY). The protein was then run on a size exclusion chromatography column (Superdex 75 16/60 High load) equilibrated with 25 mM HEPES, pH 7.4, 150 mM KCl, 0.4 mM TCEP and further purified by anionic exchange (Mono-S) chromatography. All chromatography was carried out with AKTA (GE Healthcare, Marlborough, MA). The protein concentration was determined with a Bradford assay using BSA as a standard.

The 260 nm/280 nm ratios were measured to check nucleotide contamination. The protein was flash frozen and stored at -80˚C with 20% glycerol.

2.2. Surface forces measurements

The force-distance measurements were done with a home-built SFA similar to the original Israelachvili design [27]. Briefly, back-silvered mica surfaces were glued on cylindrical glass disks (R ~ 2 cm) with UV-cured glue (NOA81, Norland Optics), then a monolayer of 1,2-dimyristoyl-sn-glycero-3-phosphoethanolamine (DMPE) was deposited on both surfaces at an area/molecule of 0.4 nm^2 using a home-built Langmuir-Blodgett trough [28]. DMPE binds strongly to mica, creating a stable inner monolayer on both surfaces. Next, on one surface we deposited an outer layer of 95% 1-palmitoyl-2-oleoyl-sn-glycero-3-phosphocholine (POPC) and 5% 1,2-dioleoyl-sn-glycero-3-[(N-(5-amino-1carboxypentyl)iminodiacetic acid)succinyl] nickel (DGS-NTA-Ni) with an area/molecule of 0.4 nm^2, and on the other surface an outer layer of 80% POPC, 15% 1,2-dioleoyl-sn-glycero-3-phospho-L-serine (DOPS), and 5% L-α-phosphatidylinositol-4,5-bisphosphate (PIP2) was deposited at 0.5 nm^2. The POPC/DOPS/PIP2 membrane was kept immersed in 25 mM HEPES, 150 mM KCl, with 0.5 mM of EGTA, and in certain cases, 0.5 mM of free Ca^{2+} or 1.0 mM of free Mg^{2+} buffer (calculated using Maxchelator, maxchelator.stanford.edu).

The 95% POPC, 5% DGS-NTA-Ni membrane was immersed in a small vial of the same buffer (~3 mL volume) into which ~5 uL of ~2 mg/mL 12xHis-Syt1 was injected and mixed well via pipet. After 1 hr of protein immersion, the small vial was transferred twice into clean buffer solution (~200 mL volume) to remove unbound protein. Finally both surfaces were carefully transferred under buffer into the SFA chamber. One surface was mounted on a spring with the other on a stiff mount in a crossed-cylinder geometry. The distance was measured via multiple beam interferometry and the force by spring deflection. For each condition we measured at least 3 independent experimental setups, with at least 8 independent contact locations and at least 2 different protein batches to demonstrate reproducibility. Error bars represent standard errors over the independent contact locations.

3. Results

3.1. Effect of anionic lipids on Syt1 interactions with lipid membranes

We measured the forces during approach and separation of a Syt1-decorated membrane and an anionic membrane. In the Syt1-membrane, accounting for 5% Ni-NTA and 2-3 histidines binding per Ni-NTA gives a maximum surface density of ~2.5×10^{16} molecules of Syt1 per m^2 corresponding to ~40 nm^2/Syt1 molecule or ~1.3 Syt1 copies per every 100 lipids in the outer leaflet. As such, the experiment simulates a synaptic vesicle approaching the anionic plasma membrane, albeit in the absence of SNAREs and other regulatory proteins, in order to isolate the pure Syt1-membrane interactions.

An SFA measurement consists of approaching and separating the surfaces while measuring the distance interferometrically (distance resolution ~1 Å) and measuring the corresponding forces with a cantilever spring (force resolution ~100 nN). In the standard procedure, we apply a 1 hr contact time (t_c = 1 hr) between the end of the approach and the beginning of the separation, with shorter t_c in specific cases. The surfaces are approached and separated quasi-statically, such that the distance and force are measured simultaneously every ~10 s. The average speed of approach/separation outside of the interaction zone (i.e. D > 50 nm) is ~1 nm/sec, which captures the quasi-equilibrium interaction force profile between Syt1 and the opposing membrane. The surfaces were initially immersed in 150 mM KCl, 25 mM HEPES buffer, and 0.5 mM EGTA. To first examine the effects of anionic lipids on the binding of Syt1 to membranes, we adjusted the composition of the opposing "target" membrane. We measured the force-distance interactions of Syt1 approaching an anionic (PS/PIP2) membrane surface, and compared these interactions with Syt1 approaching a neutral (100% POPC) membrane surface (Fig. 2). By convention, repulsive forces have a positive sign while attractive forces have a negative sign.

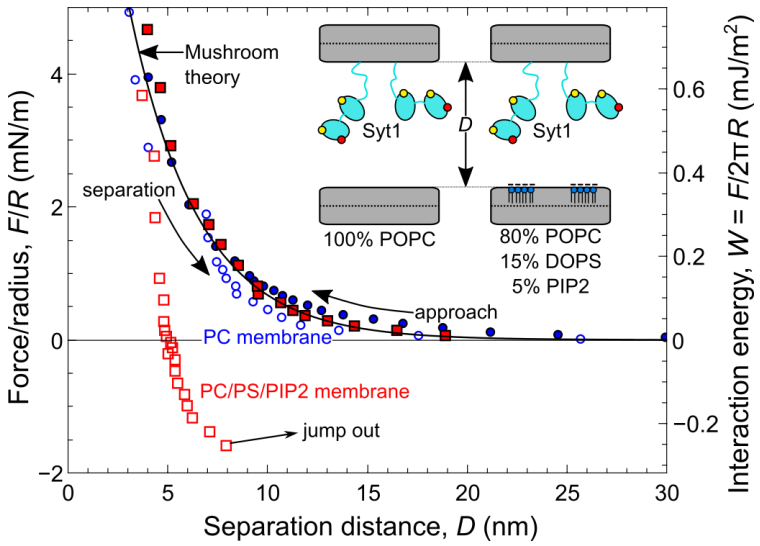

Figure 2. Interaction force vs. distance measurement (approach and separation) by SFA for Syt1 membrane with a 100% POPC membrane (blue circles), and a Syt1-coated membrane with an 80% POPC, 15% DOPS, and 5% PIP2 membrane (red squares). Filled symbols are during approach while empty symbols are during separation. In the Syt1-membrane cartoons (upper right), the Ca^{2+} binding loops of C2A and C2B are indicated by the yellow sites, and the polybasic patch on C2B is indicated by the red site.

During the approach of Syt1, a significant force was first measured at D ~ 25-30 nm, which roughly corresponds to the fully stretched Syt1 [29]. Electrostatic interactions at this range are vanishingly small (Debye length ~0.8 nm), so this interaction is attributed to a steric interaction between the Syt1 chains and the anionic membrane surface. As the surfaces are pushed further together (a primitive mimic of the SNARE/Munc13 complex which brings the vesicle and plasma membrane together from large distances), an exponential repulsion is measured. These observations indicate that in spite of the structured C2A and C2B domains, the 61-residue linker between the transmembrane domain and C2A combined with the 9-residue linker between C2A and C2B are unstructured when not under confinement, and the isolated protein behaves similar to a random coil. We therefore apply the polymer mushroom model, which has also been applied to SNARE proteins [30],

$$F/R = 72\pi\Gamma k_B T e^{-\sqrt{3}D/R_g}, \quad (1)$$

where F is the measured force, R ~ 2 cm is the radius of the surfaces, Γ is the surface density of Syt1, k_B is Boltzmann's constant, T = 298 K is the temperature, D is the distance between the

membranes (see Fig. 1), and R_g is the radius of gyration of Syt1. By fitting this equation to the measured F/R vs. D curves, we measure Γ and R_g.

The approach curves (filled points, Fig. 2) are nearly equivalent for both the PC membranes and the anionic membranes, revealing that the long-range interactions between Syt1 and membranes do not depend on the membrane charge. These repulsive forces follow the mushroom model closely, and the measurement reveals a surface coverage Γ ~1x10^{16} molecules/m^2 and radius of gyration R_g ~6±0.5 nm for both conditions (Fig. 2, black curve). However, upon separating the two surfaces, drastic differences are observed between the PC lipids and anionic lipid membranes. For the PC membrane, a small hysteresis is measured (compared to the approach curve), but no adhesion is observed. This suggests that the Syt1 molecules are in a slightly compressed mode upon separation, but they do not bind specifically to the PC lipids. Conversely, for the anionic membrane, a strong adhesion force F_{ad} is measured, as the force at which the spring experiences an instability and a so-called jump-out of contact is observed (indicated by the "jump-out" arrow in Fig. 2). By applying Derjaguin's Approximation, which is valid for $R >> D$ and if the interactions decrease at least as $1/D^2$ (and when the surfaces are not deformed or flattened), we find the surface energy per unit area, W, as

$$W = \frac{F}{2\pi R} \quad . \tag{2}$$

The normalized adhesion force is measured as F_{ad}/R = -1.6 mN/m, corresponding to an adhesion energy W_{ad} = -0.25 mJ/m^2. Then, using this adhesion energy, one can find the energy per molecule of Syt1, by

$$E_{\mathrm{Syt1}} = W/\Gamma \quad . \tag{3}$$

As such, we measure the energy per molecule as a function of distance between the membranes, allowing for distance-dependent probing of the energetics of confinement and binding of Syt1. In the case of Syt1 binding to the anionic lipid membrane in 0.5 mM EGTA, W_{ad} = -0.25 mJ/m^2 and Γ = 1.3x10^{16} molecules/m^2 give a binding energy E_{Syt1}~5 k_BT. These values were taken from the force-distance measurement presented in Fig. 2. Calculating the average and standard error over a representative sample of 8 independent measurements gives E_{Syt1} = 5.8±0.9 k_BT in EGTA. Note that the sign of the binding energy is reported as positive by convention as the magnitude of the adhesion (*i.e.*, negative) force and energy.

3.2. Effects of divalent cations Mg^{2+} and Ca^{2+} on Syt1 interactions with lipid membranes

Next, we measured energy vs. distance curves separately in 0.5 mM EGTA, 0.5 mM free Mg^{2+}, and 0.5 mM free Ca^{2+}, to examine the effects of Mg^{2+} and Ca^{2+} on the interaction between Syt1 and the anionic membrane (Fig. 3). As Syt1 approaches the membrane, an exponential repulsive force profile was observed again (Fig. 3A,B), which closely follows the mushroom model with R_g = 6±0.5 nm in all 3 cases (Fig. 3B), indicating that the divalent ions do not have a significant effect on the extended structure before Syt1 contacts the membrane. The surfaces are driven together until F/R ~5 mN/m, where the distance remaining between the bilayers is D = 5.2±0.3 nm (*i.e.*, the confined Syt1 thickness), a similar value to thicknesses previously measured for Syt1 bridging between liposomes [8,10,29,31]. As observed by the repulsive interactions (Fig. 3A,B), confining Syt1 to this level has an energetic cost of ~15-20 k_BT. This energy might be overcome by binding to SNAREs or Munc13 *in vivo*, or if Syt1 localizes away from the center of the contact zone of the highly curved vesicle, then this barrier could be significantly lower.

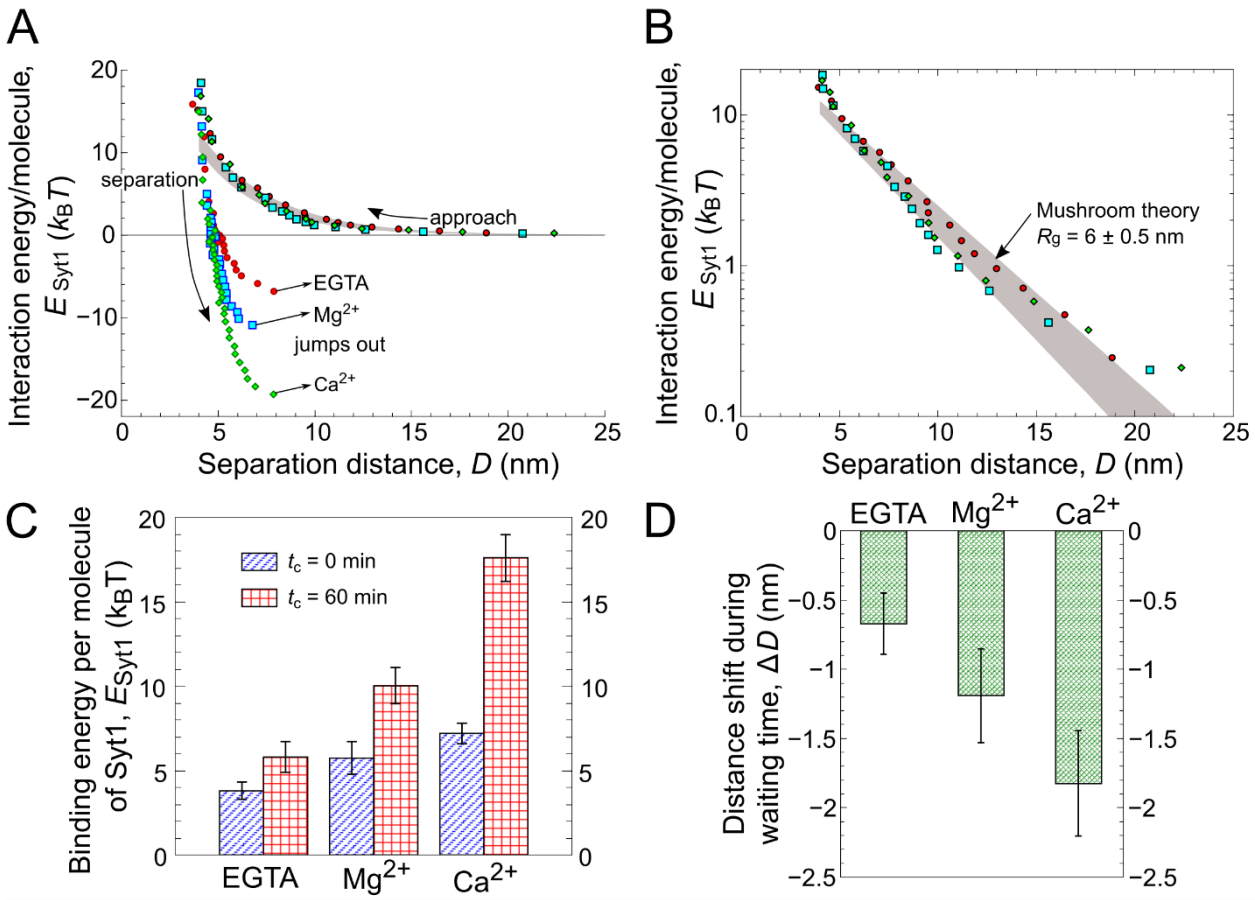

Figure 3. Force-distance measurements by SFA in the presence of EGTA, Mg^{2+}, and Ca^{2+} for (A) approach and separation on normal axes and (B) approach forces only on a semilog plot. (C) Summary of binding interactions at short and long contact times, and (D) summary of the distance shift during the 1 hr contact time for each condition.

Figure 3A,B shows selected force runs; every individual measurement results in a measurement of Γ, R_g, W_{ad}, and therefore E_{Syt1}. Typically, Γ ranges from about ~5x10^{15} to ~2x10^{16} molecules/m^2, while R_g is in the range 5-8 nm. When the surfaces are separated from each other, divalent ions lead to significant increases to the binding energy (Fig. 3A,C). Addition of Ca^{2+} is known to cause insertion of the hydrophobic residues near the Ca^{2+} binding sites of C2AB, and the binding energy increases to E_{Syt1} = 17.6 ± 1.4 k_BT. Notably, the binding increases in Mg^{2+}, from E_{Syt1} = 5.8 ± 0.9 k_BT in EGTA to E_{Syt1} = 10.0 ± 1.1 k_BT in Mg^{2+}. This increase in the binding energy implicates interaction of the hydrophobic loops when Syt1 coordinates Mg^{2+}, likely due to a weaker hydrophobic loop interaction compared to Ca^{2+} (see discussion for details). An experiment

performed in buffer containing 0.5 mM free Ca^{2+} and 1 mM free Mg^{2+} gave nearly identical results to the energy measured in Ca^{2+} alone, with E_{Syt1} = 16.1 ± 2.1 k_BT.

The binding energies at short contact times, t_c = 0 min, were also measured, as shown in Figure 3C. These results show the same trend as the binding energies for t_c = 60 min, although the trend is less pronounced. The experiment performed in 0.5 mM free Ca^{2+} and 1 mM free Mg^{2+} gave E_{Syt1} = 7.9 ± 0.9 k_BT for t_c = 0 min, again virtually the same as the value measured in Ca^{2+} alone (E_{Syt1} = 7.2 ± 0.6 k_BT). The binding kinetics, which plateau between t_c = 30-60 min, are shown in supporting information (Section S1). Syt1 triggers Ca^{2+} dependent fusion remarkably quickly *in vivo*, often in less than a millisecond [2]. The slow equilibration in the SFA measurement, over the course of ~1 hr, is clearly non-biological. This timescale for equilibration was also observed for SNARE proteins [30] and is likely due to the surface geometry, which provides confinement to nm-level distances over hundreds of μm^2 compared to hundreds of nm^2 in the synaptic vesicle. However, the slow kinetics are in fact advantageous in the present measurements because it enables observation of slow molecular rearrangements. This confinement effect may be enhanced by the Syt1 concentration which is around 10x larger than the average Syt1 content of a synaptic vesicle [32]. Nonetheless, if all Syt1 are bound to the plasma membrane, *e.g.* as in the recently proposed ring-shaped oligomers model [19], their local concentration is increased up to the same order of magnitude as the concentration in the current SFA experiments. In any case, using 10x smaller Syt1 concentration in the present measurements would decrease the magnitudes of Γ and W_{ad} accordingly, making accurate measurement of E_{Syt1} impossible.

By measuring the distance at the final point of approach and first point of separation at the same applied force, we obtain the distance shift during the contact time, $\Delta D = D_{separation,initial} - D_{approach,final}$, as shown in detail in the supporting information (Section S2). A negative value for ΔD indicates an inward distance shift (*i.e.*, the surfaces become closer together). For t_c = 0 min, ΔD is zero within experimental error. However, for t_c = 1 hr, ΔD increases in magnitude from -0.7 nm in EGTA, to -1.2 nm in Mg^{2+}, and to -1.8 nm in Ca^{2+}, as shown in Figure 3D. Therefore, the binding energies were correlated with ΔD, indicating that relatively slow molecular rearrangements during confinement lead to the increased adhesion, discussed in more detail below.

4. Discussion

Most previous measurements of Syt1-membrane binding have utilized only the soluble C2AB to measure association with a membrane. Importantly, we include the entire cytoplasmic portion of Syt1 and attach it directly to a membrane, providing a more precise mimic of Syt1 in synaptic vesicles approaching the plasma membrane. Under physiological conditions, the Syt1 interaction with *cis* PS lipids is known to be screened by ATP, such that only the *trans* interaction is productive [26]. Therefore, by including only PC in the *cis* membrane, we measure the Syt1-*trans* interaction under the physiologically-relevant topology.

Previous solution phase measurements indicate that Ca^{2+}-independent binding of C2AB to anionic membranes occurs through the C2B polylysine patch, while the C2A plays a small or negligible role in lipid binding [5,7,23]. Therefore, the adhesion measured here between Syt1 and the anionic membrane in EGTA, $E_{Syt1} = 5.8 \pm 0.9\ k_BT$, likely arises primarily from the binding of the polylysine patch of C2B with the anionic PS and PIP2 lipid headgroups. Several groups have measured association or dissociation constants via isothermal calorimetry or MST, which can be used to calculate a binding free energy. With similar lipid compositions the dissociation constant measurements of Syt1 with membranes are reported to be in the range of ~5-10 k_BT in EGTA [6,7]. A recent single molecule study reported no binding between C2AB and an anionic membrane in the absence of Ca^{2+}, possibly because the Ca^{2+}-independent binding requires participation of multiple molecules [20]. The value reported here ($5.8 \pm 0.9\ k_BT$) is in the lower range of values reported thus far, which is perhaps expected. By including the entire cytosolic domain and anchoring it to a membrane, we have reduced degrees of freedom compared to the solution phase measurements. Similarly, the extreme confinement due to the close apposition of both membranes reduces the degrees of freedom for Syt1 even further and provides a model closer to the crowded and confined situation *in vivo*.

A simple screened Coulomb interaction to model the polybasic patch as a cation of valence +4 and the PIP2 as an anion of valence -3 allows for a simplified view of this interaction. As shown in the supporting information (Section S3), this ion-ion interaction is fully attractive but becomes significant compared to the thermal energy only for separations ~1 nm. The contact energy (*i.e.*, adhesion or binding energy) is ~8 k_BT. A combined experimental-theoretical study of polylysine binding at anionic membrane surfaces found that each lysine provided about 1.7 k_BT to the total

binding energy [33], such that a 4-lysine stretch as found in C2B should bind with ~7 k_BT. These simplified models are in rough agreement with the experimentally measured value, indicating that the C2B-membrane interaction is almost purely accounted for as a charge-charge interaction between the polybasic patch and the anionic lipids.

The increased binding of Syt1 in the presence of Ca^{2+} is also expected from previous work [9,20], which indicates that Syt1 reorients to insert the hydrophobic residues of the Ca^{2+} loop into the membrane. A recent optical tweezers study reported a binding energy of ~12 k_BT in the presence of 0.5 mM free Ca^{2+} for C2AB binding to an anionic membrane [20]. A wide range of dissociation constants, and therefore binding energetics, have been measured by traditional biological assays for soluble C2AB with anionic membranes, with a maximum value of ~25 k_BT [9]. The value measured here in 0.5 mM Ca^{2+}, $E_{Syt1} = 17.6 \pm 1.4$, is again smaller than the traditional assays, although is potentially more representative physiologically because Syt1 is anchored to the membrane.

The increase in the binding energy upon addition of Mg^{2+} (compared to in EGTA) has not been previously reported and is potentially due to a weaker interaction of the Ca^{2+} binding pocket in the presence of Mg^{2+} that results in partial insertion of the hydrophobic loops. The membrane binding energy in Mg^{2+} is between the binding energies measured in Ca^{2+} and EGTA. One possible explanation for the weaker overall interaction in Mg^{2+} compared to Ca^{2+} is that partial hydrophobic loop insertion occurs in concert with binding of the polybasic patch. The other possibility is that the polybasic patch is no longer bound in the presence of Mg^{2+} and the binding energy originates entirely from the partial loop insertion. These possibilities are presented schematically in Figure 4 and discussed further directly below. We cannot distinguish between these in the current measurements and more detailed structural measurements could help elucidate the mechanism. Since we obtained similar binding energies for experiments in Ca^{2+} and both Ca^{2+} and Mg^{2+} simultaneously, it appears that the Mg^{2+} occupies the Ca^{2+} sites in the absence of Ca^{2+}, but Ca^{2+} outcompetes Mg^{2+} when they are both present, such that Syt1 reaches the full Ca^{2+}-dependent binding energy.

Due to the geometry in the SFA, the first Syt1-membrane interaction is through the C2B polybasic patch which orients the C2B and provides a similar initial binding conformation in all 3 conditions, as shown in Figure 4. The measurements of ΔD indicate that Syt1 molecules slowly

rearrange to find their final conformation. Even for t_c=0 min, the surfaces remain at ~5 nm level confinement for ~5 minutes, allowing some small fraction of molecules to change conformation and leading to the observed adhesion increase for the t_c=0 min case over the 3 conditions. In EGTA, the small increase in binding energy over t_c=1 hr combined with the small value for ΔD implicate non-specific rearrangements. In Ca^{2+}, the C2B hydrophobic loops prefer an upright orientation during loop insertion, allowing C2A to rotate and align parallel with the C2B during the equilibration to insert its hydrophobic loops in the membrane, leading to the measured large increase in binding and more dramatic rearrangements of ΔD = -1.8 nm in Ca^{2+}. With Mg^{2+}, the C2B again contacts the membrane first via the C2B polybasic patch, with the additional possibility of partial loop insertion. Rotation during the contact time results in a similar side-by-side configuration of C2AB, but due to only partial hydrophobic loop insertion, the distance shift is limited to ΔD = -1.2 nm and the binding energy increase is modest.

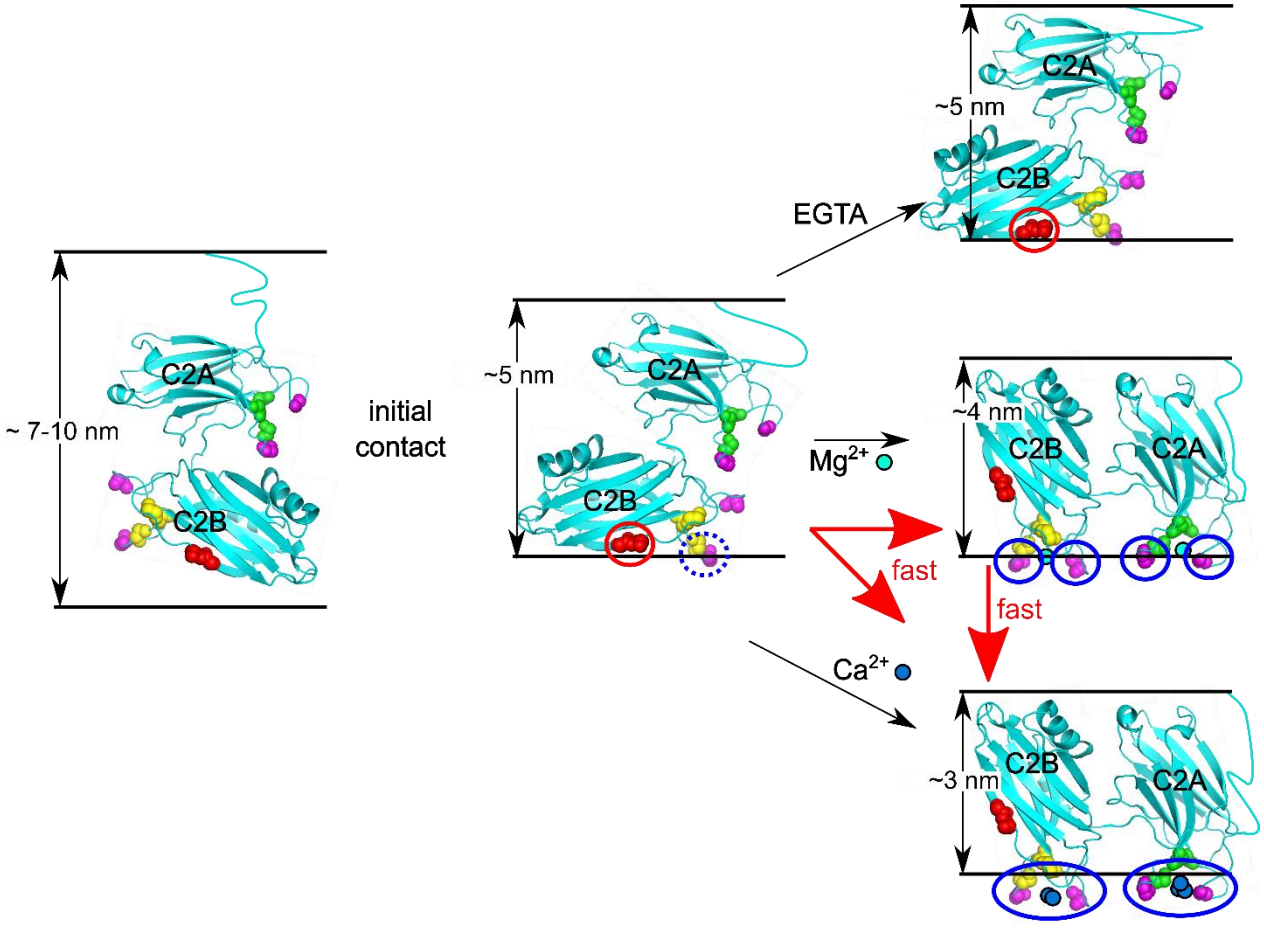

Figure 4. Schematic mechanism for the Syt1-membrane rearrangements measured in this study. The Syt1 is anchored to the top membrane. Important residues of Syt1 are labeled as follows: red,

C2B polybasic; yellow, C2B Ca^{2+} binding; green, C2A Ca^{2+} binding; pink, C2A and C2B hydrophobic loops. Membrane contacts are denoted by red circles (polybasic patch), blue circles (partial hydrophobic loop insertion), blue ovals (full hydrophobic loop insertion). Black arrows denote the slow measured rearrangements (over the course of 1 hr), while hypothesized fast (~msec) potential physiological transitions are denoted by the heavy red arrows (labeled "fast"). See text for detailed mechanistic explanation.

With a physiological concentration of ~1 mM Mg^{2+}, the measurements in Mg^{2+} potentially reveal mechanisms of Syt1 action. Several previous studies have suggested that the presence of Mg^{2+} is important for the Ca^{2+} sensitivity of Syt1 [22–24]. Rearrangements of potential physiological importance measured here include the transition from polybasic patch binding, to partial loop insertion in Mg^{2+}, to full loop insertion in Ca^{2+} (Fig. 4). Additionally, if C2A is held adjacent to the *cis* membrane by SNAREs or other conformational factors, the rearrangement from C2B polybasic binding/partial loop insertion in Mg^{2+} to full loop insertion in Ca^{2+} may be physiologically relevant. These rearrangements are not necessarily sequential and might be multimodal such that during loop insertion, the polybasic patch interaction persists to some degree [9]. Prior to fusion, the partial loop insertion in Mg^{2+} potentially places the Syt1 just at the edge of the required conformational change in order to facilitate fast kinetics in Ca^{2+}. While these measurements are consistent with the ring model [16,18,19], no direct evidence of Syt1 rings or oligomers was found. It is difficult to envision how oligomerization would impact the measured results in SFA. While the slow rearrangements might reflect oligomerization, they also simply might be an effect of the large scale confinement over many μm^2. Similarly, the measured R_g is ~2-3x larger than the expected R_g for Syt1 [34,35], which could be a subtle signature of oligomerization, but also might simply result from differences between measuring R_g for the full cytoplasmic domain between 2 surfaces (as done here) *vs*. measuring R_g of C2AB in solution. Importantly, the transition from the initial contact state in Mg^{2+} to the equilibrated loop insertion in Ca^{2+} is consistent with the ring model.

We directly measured Syt1-membrane binding energies and interaction mechanisms, along with confinement and molecular rearrangement details of Syt1-membrane interactions. Future measurements focusing on Syt1 mutants and more realistic lipid compositions will help to precisely assess the roles of different Syt1 binding sites. While the current results suggest that the hydrophobic loops play a role in the presence of Mg^{2+}, additional structural and biochemical work

is required to elucidate the precise nature of this interaction. The inclusion of SNAREs and observation of Syt1 loop-insertion, in correlation with measurements of distance-dependent binding energetics, could help elucidate the precise mechanistic details of Syt1 action in fast Ca^{2+}-triggered synaptic transmission.

ACKNOWLEDGEMENTS

This work was supported by Agence Nationale de la Recherche (ANR) ANR-14-1CHN-0022-01 to JER. CG was supported by the Fondation pour la Recherche Médicale (FRM) FDT20170437276. SHD was supported by LabEX ENS-ICFP: ANR-10-LABX-0010/ANR-10-IDEX-0001-02 PSL*.

REFERENCES

1 Chapman ER (2002) Synaptotagmin: A Ca2+ sensor that triggers exocytosis? *Nat. Rev. Mol. Cell Biol.* **3**, 498–508.

2 Südhof TC & Rothman JE (2009) Membrane fusion: Grappling with SNARE and SM proteins. *Science (80-.).* **323**, 474–477.

3 Brose N, Petrenko AG, Südhof TC & Jahn R (1992) Synaptotagmin: a calcium sensor on the synaptic vesicle surface. *Science* **256**, 1021–1025.

4 Martens S, Kozlov MM & McMahon HT (2007) How Synaptotagmin Promotes Membrane Fusion. *Science (80-.).* **316**, 1205–1208.

5 Bai J, Tucker WC & Chapman ER (2004) PIP2 increases the speed of response of synaptotagmin and steers its membrane-penetration activity toward the plasma membrane. *Nat. Struct. Mol. Biol.* **11**, 36–44.

6 Den Van Bogaart G, Meyenberg K, Diederichsen U & Jahn R (2012) Phosphatidylinositol 4,5-bisphosphate increases Ca2+ affinity of synaptotagmin-1 by 40-fold. *J. Biol. Chem.* **287**, 16447–16453.

7 Kuo W, Herrick DZ, Ellena JF & Cafiso DS (2009) The Calcium-Dependent and Calcium-Independent Membrane Binding of Synaptotagmin 1: Two Modes of C2B Binding. *J. Mol. Biol.* **387**, 284–294.

8 Araç D, Chen X, Khant HA, Ubach J, Ludtke SJ, Kikkawa M, Johnson AE, Chiu W, Südhof TC & Rizo J (2006) Close membrane-membrane proximity induced by Ca2+-dependent multivalent binding of synaptotagmin-1 to phospholipids. *Nat. Struct. Mol. Biol.* **13**, 209–217.

9 Pérez-Lara A, Thapa A, Nyenhuis SB, Nyenhuis DA, Halder P, Tietzel M, Tittmann K, Cafiso DS & Jahn R (2016) PtdInsP2 and PtdSer cooperate to trap synaptotagmin-1 to the plasma membrane in the presence of calcium. *Elife* **5**, 1–22.

10 Kuo W, Herrick DZ & Cafiso DS (2011) Phosphatidylinositol 4,5-bisphosphate alters

synaptotagmin 1 membrane docking and drives opposing bilayers closer together. *Biochemistry* **50**, 2633–2641.

11 Hui E, Bai J & Chapman ER (2006) Ca2+ Triggered Simultaneous Membrane Penetration of the Tandem C2-Domains of Synaptotagmin I. *Biophys. J.* **91**, 1767–1777.

12 Herrick DZ, Sterbling S, Rasch KA, Hinderliter A & Cafiso DS (2006) Position of synaptotagmin I at the membrane interface: Cooperative interactions of tandem C2 domains. *Biochemistry* **45**, 9668–9674.

13 Mackler JM, Drummond JA, Loewen CA, Robinson IM & Reist NE (2002) The C(2)B Ca(2+)-binding motif of synaptotagmin is required for synaptic transmission in vivo. *Nature* **418**, 340–344.

14 Paddock BE, Wang Z, Biela LM, Chen K, Getzy MD, Striegel A, Richmond JE, Chapman ER, Featherstone DE & Reist NE (2011) Membrane Penetration by Synaptotagmin Is Required for Coupling Calcium Binding to Vesicle Fusion In Vivo. *J. Neurosci.* **31**, 2248–2257.

15 Hui E, Johnson CP, Yao J, Dunning FM & Chapman ER (2009) Synaptotagmin-Mediated Bending of the Target Membrane Is a Critical Step in Ca 2 + -Regulated Fusion. *Cell* **138**, 709–721.

16 Wang J, Bello O, Auclair SM, Wang J, Coleman J, Pincet F, Krishnakumar SS, Sindelar C V. & Rothman JE (2014) Calcium sensitive ring-like oligomers formed by synaptotagmin. *Proc. Natl. Acad. Sci. U. S. A.* **111**, 13966–71.

17 Zanetti MN, Bello OD, Wang J, Coleman J, Cai Y, Sindelar C V, Rothman JE & Krishnakumar SS (2016) Ring-like oligomers of Synaptotagmins and related C2 domain proteins. *Elife* **5**, 1–15.

18 Wang J, Li F, Bello OD, Sindelar CV, Pincet F, Krishnakumar SS & Rothman JE (2017) Circular oligomerization is an intrinsic property of synaptotagmin. *Elife* **6**, 1–17.

19 Rothman JE, Krishnakumar SS, Grushin K & Pincet F (2017) Hypothesis: Buttressed Rings Assemble, Clamp, and Release SNAREpins for Synaptic Transmission. *FEBS Lett.* **591**, 3459–3480.

20 Ma L, Cai Y, Li Y, Jiao J, Wu Z, O'Shaughnessy B, Karatekin E, De Camilli P & Zhang Y (2017) Single-molecule force spectroscopy of protein-membrane interactions. *Elife* **6**, 1–21.

21 Takahashi H, Shahin V, Henderson RM, Takeyasu K & Edwardson JM (2010) Interaction of synaptotagmin with lipid bilayers, analyzed by single-molecule force spectroscopy. *Biophys. J.* **99**, 2550–2558.

22 Zhou Q, Lai Y, Bacaj T, Zhao M, Lyubimov AY, Uervirojnangkoorn M, Zeldin OB, Brewster AS, Sauter NK, Cohen AE, Soltis SM, Alonso-Mori R, Chollet M, Lemke HT, Pfuetzner RA, Choi UB, Weis WI, Diao J, Südhof TC & Brunger AT (2015) Architecture of the synaptotagmin–SNARE machinery for neuronal exocytosis. *Nature* **525**, 62–67.

23 Schiavo G, Gu QM, Prestwich GD, Söllner TH & Rothman JE (1996) Calcium-dependent switching of the specificity of phosphoinositide binding to synaptotagmin. *Proc. Natl. Acad.*

Sci. **93**, 13327–13332.

24 Lee H, Yang Y, Su Z, Hyeon C, Lee T, Lee H, Kweon D-H, Shin Y-K & Yoon T-Y (2010) Dynamic Ca2+ Dependent Stimulation of Vesicle Fusion by Membrane-Anchored Synaptotagmin 1. *Science (80-.).* **328**, 760–763.

25 Stein A, Radhakrishnan A, Riedel D, Fasshauer D & Jahn R (2007) Synaptotagmin activates membrane fusion through a Ca2+-dependent trans interaction with phospholipids. *Nat. Struct. Mol. Biol.* **14**, 904–911.

26 Park Y, Hernandez JM, Van Den Bogaart G, Ahmed S, Holt M, Riedel D & Jahn R (2012) Controlling synaptotagmin activity by electrostatic screening. *Nat. Struct. Mol. Biol.* **19**, 991–999.

27 Israelachvili JN & Adams GE (1978) Measurement of forces between two mica surfaces in aqueous electrolyte solutions in the range 0-100 nm. *J. Chem. Soc. Faraday Trans. 1* **74**, 975.

28 Perez E & Wolfe J (1994) A simple, Cheap, Clean, Reliable, Linear, Sensitive, Low-Drift Transducer for Surface Pressure. *Langmuir* **10**, 974–975.

29 Lin C, Seikowski J, Pérez-Lara A, Jahn R, Höbartner C & Walla PJ (2014) Control of membrane gaps by synaptotagmin-Ca2+ measured with a novel membrane distance ruler. *Nat. Commun.* **5**, 5859.

30 Li F, Pincet F, Perez E, Eng WS, Melia TJ, Rothman JE & Tareste D (2007) Energetics and dynamics of SNAREpin folding across lipid bilayers. *Nat. Struct. Mol. Biol.* **14**, 890–896.

31 Seven AB, Brewer KD, Shi L, Jiang Q-X & Rizo J (2013) Prevalent mechanism of membrane bridging by synaptotagmin-1. *Proc. Natl. Acad. Sci.* **110**, E3243–E3252.

32 Takamori S, Holt M, Stenius K, Lemke EA, Grønborg M, Riedel D, Urlaub H, Schenck S, Brügger B, Ringler P, Müller SA, Rammner B, Gräter F, Hub JS, De Groot BL, Mieskes G, Moriyama Y, Klingauf J, Grubmüller H, Heuser J, Wieland F & Jahn R (2006) Molecular Anatomy of a Trafficking Organelle. *Cell* **127**, 831–846.

33 Ben-Tal N, Honig B, Peitzsch RM, Denisov G & McLaughlin S (1996) Binding of small basic peptides to membranes containing acidic lipids: theoretical models and experimental results. *Biophys. J.* **71**, 561–575.

34 Guan Z, Bykhovskaia M, Jorquera RA, Sutton RB, Akbergenova Y & Littleton JT (2017) A synaptotagmin suppressor screen indicates SNARE binding controls the timing and Ca2+cooperativity of vesicle fusion. *Elife* **6**, 1–30.

35 Liu H, Bai H, Xue R, Takahashi H, Edwardson JM & Chapman ER (2014) Linker mutations reveal the complexity of synaptotagmin 1 action during synaptic transmission. *Nat. Neurosci.* **17**, 670–677.